Mesoscale modelling with the Lattice Boltzmann Method

Jonathan Chin <j.chin@qmw.ac.uk>
Department of Chemistry, Queen Mary, University of London

Supervisor: Prof. P. V. Coveney

June 6, 2001

Contents

0.1 Summary

The lattice Boltzmann equation (LBE) method is a relatively new procedure for computational modelling of fluid dynamics, and in particular, modelling of mesoscale effects. A brief account of why mesoscale phenomena are worth looking at is given, followed by a review of the literature surrounding LBE and its application to mesoscale modelling.

A report is then presented into an investigation of spinodal decomposition with LBE techniques, including some basic theory surrounding the process and comparison of the results obtained from LBE simulations to the theoretical predictions.

0.2 Statement of Attendance

0.2.1 Lecture Courses

- **Parallel Computing C1(a)**
  Dr. D. R. Moore, Imperial College, Autumn 2000
- **Safety and COSHH Regulations**
  26/9/2000
- **ISI Science Citation Index**
  5/10/2000
- **Chemical Abstracts & other Lit. Databases**
  6/10/2000
- **Scientific Writing**
  27/10/2000
- **Oral Presentations**
  1/12/2000

0.2.2 Seminars

- **Modelling and Simulation of Turbulent Flow**
  Prof. Bernard J. Geurts , University of Twente, The Netherlands and Queen Mary, University of London : 21/9/2000
- **Exponentially-Decaying Collision Operators**
  Dr. Oscar Bandtlow , University of Glasgow : 1/11/2000
- **Langevin Dynamics From Rescaled Deterministic Chaotic Dynamics**
  Dr. Christian Beck , Queen Mary, University of London : 9/11/2000
- **When the Temperature Gets Hot: Finite Temperature Simulations Using Density Functional Theory**
  Dr. Phil Hasnip , University of Cambridge : 16/1/2001
- **Origins of RNA and vibrations in DNA**
  Dr. Jonathan Wattis, University of Nottingham : 24/1/2001
- **Plane Wave Density Functional Theoretic Study of In Situ Copolymerisation Within Clay Minerals**
  Stephen Stackhouse , Queen Mary, University of London : 7/2/2001
- **Dynamics of Wormlike Micellar Systems**
  Dr. Octavio Manero , UNAM, Mexico: 14/2/2001
- **Kinetics of surfactant phase transitions**
  Dr Stefan Egelhaaf, University of Edinburgh : 4/4/2001

- **Particle Softness and its Influence on Molecular Viscoelasticity**
  Professor D. M. Heyes, University of Surrey : 21/2/2001
- **Inductive Logic Programming: Towards Machine Assisted Scientific Theory Formation**
  Dr. Steve Moyle, University of Oxford: 2/5/2001
- **Lattice Kinetic Schemes for Magnetohydrodynamics**
  Dr. Paul Dellar, University of Cambridge: 9/5/2001
- **Chemistry and Biology from First Principles**
  Prof. Mike Payne, University of Cambridge: 23/5/2001

Chapter 1

Literature Review

Plagiarize, plagiarize, plagiarize!
Only be sure always to call it please, "research".
– Tom Lehrer, *Lobachevsky*

1.1 Overview of Mesoscale Modelling

A brief discussion of the meaning and importance of mesoscale modelling is given, followed by a review of the literature surrounding several techniques, focussing on the lattice Boltzmann method. Although it is possible to derive lattice Boltzmann methods directly from the well-known continuum Boltzmann equation[1, 2], this is not how the method arose historically, and much useful theory pertaining to lattice Boltzmann methods arose from considerations of other techniques, particularly lattice gas automata.

1.1.1 Why is mesoscale modelling useful?

Physical science has met with much success in modelling phenomena on microscopic and macroscopic scales. A microscopic model usually considers the behaviour of every single component atom of a system; the increasing complexity of such models as the number of atoms increases tends to limit the treatable length scales to the order of nanometres; typical timescales are limited to the order of nanoseconds. For example, a microscopic view of a paramagnetic crystal would describe the magnetization of every single atom in the crystal lattice; a microscopic model of a fluid would describe the position, momentum, and rotation of every single fluid molecule; a microscopic model of a single cubic millimetre of monatomic gas at room temperature and pressure would have to deal with around 10^{17} variables.

A macroscopic model, on the other hand, usually deals with a smaller number of parameters, often more closely related to physical observables. A macroscopic view of a paramagnetic crystal would describe the nett magnetization of the entire crystal and its temperature; a macroscopic view of a fluid would describe its velocity, density and temperature at various points.

The field of Statistical Mechanics has met with much success in producing macroscopic, thermodynamic descriptions of systems from their microscopic descriptions; however, its success has been limited in cases where the system is not close to thermodynamic equilibrium. In addition, comparatively few methods exist for the treatment of systems which contain processes operating at a wide range of length scales.

Mesoscale models are intended to treat systems which have intermediate length scales, or which contain processes operating at several distinct length scales. “Complex fluids”, such as fluid mixtures, colloids, suspensions, or fluids flowing through porous media, are a good example of an area where mesoscale modelling is important, since the bulk fluid flow is an important macroscopic variable, but its behaviour is highly dependent on the microscopic behaviour of the fluid interface or suspended particles. That a mixture of cornflour and water becomes more difficult to stir when one stirs it quickly is macroscopic behaviour often observed in the kitchen, but it is due to the microscopic interaction between the tiny starch molecules in the cornflour.

1.1.2 Why is mesoscale modelling difficult?

Most scientific models deal only with a small range of length or time scales. Mesoscopic systems spanning several length scales are difficult to model microscopically, because a vast amount of effort is required, and difficult to model macroscopically, because the fine details which give rise to the characteristic behaviour of such systems are lost.

For example, the two traditional approaches to modelling the behaviour of fluids have been Molecular Dynamics (MD) simulations, where each atom in the fluid is fully described, and conventional continuum Computational Fluid Dynamics (CFD), where the Navier-Stokes equations describing the fluid are discretized and solved numerically. The former approach fails with mesoscopic fluids, since the time scales of interest range from milliseconds upwards, whereas molecular dynamics techniques struggle to reach the microsecond scale. On the other hand, CFD models cannot resolve details below the order of millimetres or milliseconds.

1.1.3 Dissipative Particle Dynamics

The Dissipative Particle Dynamics (DPD) model was originally proposed by Hoogerbrugge and Koelman[3], and models the behaviour of fictitious mesoscopic “‘particles”, each corresponding to a large number of microscopic fluid particles; the original formulation was modified slightly by Español and Warren[4], so that the model produces a Gibbsian equilibrium distribution.

The state of a DPD system is completely specified by the positions $\mathbf{r}_i$, masses m_i, and momenta $\mathbf{p}_i$ of all N constituent dissipative particles; the position and momenta are continuous, but the model uses discrete timesteps δt; each timestep consists of a collision stage and an advection stage.

In the propagation step, particles coast along according to their momentum vectors, giving

$$\dot{\mathbf{r}}_i = \frac{1}{m}\mathbf{p}_i \tag{1.1}$$

Following the notation of Español and Warren, the particle momenta are updated according to the rule:

$$\dot{\mathbf{p}}_i = \sum_{j\neq i}\mathbf{F}_{ij}^C + \sum_{j\neq i}\mathbf{F}_{ij}^D + \sum_{j\neq i}\mathbf{F}_{ij}^R \tag{1.2}$$

$\mathbf{F}_{ij}^C$ is a conservative interaction force between the dissipative particles, $\mathbf{F}_{ij}^D$ is a dissipative, viscous force, and $\mathbf{F}_{ij}^R$ is a random force; stochastic fluctuations are introduced into the model through the last term. A simple form of these forces, satisfying Galilean invariance and isotropy, and simplifying further theoretical treatment of the system, is

$$\mathbf{F}_{ij}^D = -\gamma\omega_D(r_{ij})(\mathbf{e}_{ij}\cdot\mathbf{v}_{ij})\mathbf{e}_{ij} \tag{1.3}$$
$$\mathbf{F}_{ij}^R = \sigma\omega_R(r_{ij})\mathbf{e}_{ij}\zeta_{ij} \tag{1.4}$$

where $\mathbf{e}_{ij}$ is the unit vector pointing from the jth particle to the ith particle, $\mathbf{v}_{ij}$ is the relative velocity of the particles, and ζ_{ij} is a Gaussian white noise term such that $\zeta_{ij} = \zeta_{ji}$, and with the properties that

$$\begin{aligned} \langle\zeta_{ij}(t)\rangle &= 0 \\ \langle\zeta_{ij}(t)\zeta_{i'j'}(t')\rangle &= (\delta_{ii'}\delta_{jj'} + \delta_{ij'}\delta_{ji'})\delta(t-t') \end{aligned} \tag{1.5}$$

The weighting functions ω_D and ω_R define the range of interaction for the dissipative and random forces; typically, there is no interaction beyond some cutoff radius r_c – localizing interactions in this way makes the algorithm more computationally efficient. γ, which controls the magnitude of the dissipative force, can be regarded as a frictional coefficient, and σ, controlling the amplitude of the noise, is related to the temperature k_BT of the system:

$$\sigma = (2k_BT\gamma)^{\frac{1}{2}} \tag{1.6}$$

This formulation of DPD has been shown[5] to satisfy the criterion of detailed balance, namely that the product of the transition probability of the system from a state A to another state B and the probability of obtaining state A is equal to the product of the transition probability for $B \to A$ and the probability of B:

$$W(A\to B)P(A,t) = W(B\to A)P(B,t) \tag{1.7}$$

Detailed balance can be shown to be a sufficient, but not necessary, condition for a Gibbsian equilibrium condition to exist[6]. Furthermore, an H-theorem was derived for single-component DPD[7], showing that the system will inevitably equilibrate to a Gibbsian distribution.

The DPD algorithm has been extended to cover multicomponent fluids; Coveney and Español[8], and Marsh and Coveney[9] derived detailed balance conditions and H-theorems for such models.

DPD has been used to model the separation of immiscible fluids[10], phase separation under shear[11], formation of various amphiphilic phases[12], and colloidal suspensions[13]. More recently, Español[14] proposed a variant of DPD, where the dissipative particles are regarded as cells in a Voronoi lattice, with variable masses and sizes, rather than fixed spheres; Flekkøy *et al* [15] showed that this model may be derived from Molecular Dynamics through a systematic coarse-graining procedure.

1.1.4 Real-coded Lattice Gas

Malevanets and Kapral[16] proposed a model sometimes called the "Real-coded lattice gas" method. The fluid to be simulated is divided into particles whose positions occupy sites on a regular cubic lattice; each particle has a real-valued velocity $\mathbf{v}_i$. The particles are stochastically streamed to other points on the lattice, in such a way that expectation value of a particle's displacement is given by its velocity vector.

A collision stage then takes place, redistributing the velocities of the particles at each site on the lattice. At each site, the centre of mass velocity $\mathbf{V}$ is found; the particle velocities are then transformed according to a random rotation matrix σ, which differs from site to site.

$$\mathbf{v}_i' = \mathbf{V} + \sigma(\mathbf{v}_i - \mathbf{V}) \tag{1.8}$$

This collision step can be regarded as rotating all the velocity vectors at a site around the centre-of-mass velocity, which therefore remains unchanged. Hence, the total momentum at each site remains unchanged, producing hydrodynamic behaviour, while the randomization of the velocities produces dissipative behaviour. It was also shown[17] that an H-theorem exists for this model.

Hashimoto, Chen, and Ohashi[18] extended the real-coded lattice gas technique to model binary immiscible fluids, by adjusting the rotation matrix σ for each different phase, in such a way as to make the phases repel; it was verified that this model obeyed Laplace's law, namely that the pressure difference between the inside and the outside of a droplet is inversely proportional to the droplet radius. Sakai *et al* [19] extended this model to include an amphiphilic surfactant phase, and successfully modelled the process of micelle formation.

An interesting hybrid model was developed by Malevanets and Yeomans[20], where Molecular Dynamics techniques were used to model the behaviour of a short polymer chain, and a real-coded lattice gas was coupled to the MD model to add hydrodynamic effects.

1.1.5 Lattice Gas Automata

In 1986, two papers were published – one by Frisch, Hasslacher, and Pomeau[21], and the other by Wolfram[22] – which both suggested a new method for simulating fluid flow: this method had the substantial advantages that it was unconditionally stable, in contrast to conventional CFD techniques, which can be plagued by instabilities. In addition, it used only Boolean integer operations, and was thus substantially faster and simpler to implement than systems requiring floating-point logic, and it was ideally suited to parallel computers.

A lattice gas consists of a set of particles which are constrained to lie on the sites of a regular lattice. Each point $\mathbf{r}$ on the lattice has a set of vectors $\mathbf{c}_i$ connecting it to its nearest neighbours; the velocity of each fluid particle is constrained to be one of these vectors.

During each timestep of the algorithm, lattice gas particles move to adjacent points on the lattice according to their velocity vectors; they then collide with other particles at the same site in such a way as to conserve momentum. For two indistinguishable particles colliding on the hexagonal lattice used by Frisch, Hasslacher and Pomeau, often referred to as the FHP lattice, there are three possible outcomes of a collision which preserve the initial momentum: the outcome is chosen randomly from these possibilities, with equal weights. Most lattice gas models imposed an exclusion principle, so that only one particle at a given site could have a given velocity vector at any time, giving rise to Fermi-Dirac statistics for the lattice gas particles.

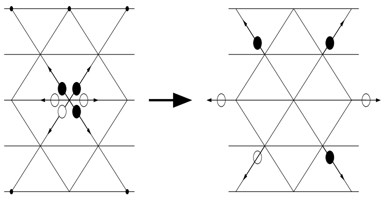

Figure 1.1: The Advection step: particles move along the lattice.

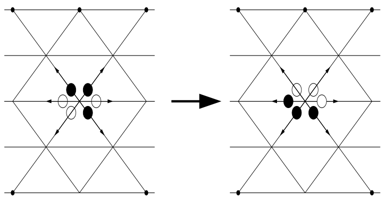

Figure 1.2: The Collision step: particles at a site are redistributed.

The discrete nature of the lattice gas model makes it a little awkward to treat analytically; the first step in most analytical treatments of LGA was to describe the algorithm in terms of the single-particle distribution function $f_i(\mathbf{r}, t)$, equivalent to the mean number of particles at position $\mathbf{r}$ with velocity $\mathbf{c}_i$. Note that f_i is a real number, in contrast to the integer occupation number n_i of the lattice gas. A lattice equivalent of the Boltzmann equation could then be found:

$$f_i(\mathbf{r} + \mathbf{c}_i, t + 1) - f_i(\mathbf{r}, t) = \Omega_i^{\sigma}(\mathbf{r}, t) \tag{1.9}$$

The left-hand side of the equation represents the advection step of the algorithm; the collision step is represented by Ω_i^{σ}, equivalent to the collision integral in the continuum Boltzmann equation.

The mean density ρ and velocity $\mathbf{u}$ of the lattice gas particles can be found from the distribution function through the relationships:

$$\rho = m \sum_i f_i \tag{1.10}$$

$$\rho u_{\alpha} = m \sum_i f_i c_{i\alpha} \tag{1.11}$$

Macroscopic equations could then be recovered for LGA by performing a Chapman Enskog procedure, similar to that which produces macroscopic equations from the continuum Boltzmann equation[23, 22, 21].

Classical fluid flow is governed by the Navier-Stokes equation: for fluid velocity $\mathbf{v}$, mass density ρ, scalar pressure p, and shear viscosity η, it states that

$$\partial_t(\rho v_{\alpha}) + \partial_{\beta}(\rho v_{\alpha} v_{\beta}) + \partial_{\alpha} p = \eta \partial_{\beta} \partial_{\beta} v_{\alpha} \tag{1.12}$$

The lattice-gas equivalent of the Navier-Stokes equation had the problem that the convection term $\partial_{\beta}(\rho v_{\alpha} v_{\beta})$ was multiplied by a density-dependent term $g(\rho)$, giving the model an unphysical lack of Galilean invariance. In addition, when the term $g(\rho)$ was not equal to unity, the model had a velocity-dependent pressure. A standard workaround for the lack of Galilean invariance was to re-scale the velocity by a factor of $1/g$; the macroscopic equations in terms of the rescaled velocity are Galilean invariant at constant density.[21]

Perhaps the most surprising result of the lattice gas models is that it is possible to model isotropic hydrodynamics on a regular lattice – it would not be unreasonable to expect that the macroscopic lattice gas fluid should tend to flow in certain specific directions determined by the underlying lattice. However, provided the lattice is chosen carefully, this does not have to be the case.

In his first paper, Wolfram constructed the nth order lattice tensor:

$$T^{(n)}_{\alpha_1 \ldots \alpha_n} \doteq \sum_i c_{i\alpha_1} \cdots c_{i\alpha_n} \tag{1.13}$$

By performing a Chapman-Enskog procedure on the lattice gas Boltzmann equation, he showed that isotropic hydrodynamics would result if the underlying lattice was isotropic to fourth order – that is to say,

$$
\begin{aligned}
T^{(1)}_{\alpha} &= 0 && (1.14)\\
T^{(2)}_{\alpha\beta} &= c_s^2 \delta_{\alpha\beta} && (1.15)\\
T^{(3)}_{\alpha\beta\gamma} &= 0 && (1.16)\\
T^{(4)}_{\alpha\beta\gamma\delta} &= c_s^4 \left(\delta_{\alpha\beta}\delta_{\gamma\delta} + \delta_{\alpha\delta}\delta_{\beta\gamma} + \delta_{\alpha\gamma}\delta_{\beta\delta}\right) && (1.17)
\end{aligned}
$$

If the lattice obeys these constraints, then lattice-effects will wash out on the macroscopic scale, and the fluid has no preferred directions. The simplest two-dimensional lattice obeying these constraints is the hexagonal FHP lattice; although no fourth-order isotropic three-dimensional regular lattice exists, it is possible to perform a lattice-gas simulation using a four-dimensional face-centred hypercubic lattice (the "FCHC" lattice), and project it down to three dimensions.

Since the LGA algorithm is concerned with tracking a finite number of discrete particles around a lattice, and is based around Boolean operations, rather than any floating-point numerical calculation, it is unconditionally stable. In addition, an H-theorem was proved by Hénon[24], showing that the Boltzmann equation describing the evolution of the occupation probabilities for each site on the lattice would inexorably evolve towards an equilibrium state.

Rothman and Keller[25] proposed an extension of the model to immiscible fluids, where, during the stochastic collision stage, outcomes resulting in the separation of lattice gas particles with differing "colour" were favoured; the model was found to obey Laplace's law. It was later shown by Boghosian and Coveney[26] that, provided the ratio of the mean free path to interaction range was small, the Rothman-Keller model could be interpreted as representing the leading-order term in an expansion of the interaction potential.

It should be noted that, even when including the interactions required to produce immiscibility, the lattice-gas algorithm is such that the state of a site at each timestep depends only on the states of that site and its nearest neighbours in the previous timestep.

Lattice gases have been generalised to model amphiphilic fluids[27], domain growth during phase separation[28], phase separation under shear[29],and flow through porous media[30, 31].

At first, lattice-gas methods appeared to offer a universal solution to the modelling of turbulent or multiphase flows, or many other problems which could not be treated with existing techniques. However, they were eventually found to suffer from several drawbacks. Although single-phase lattice-gas in two dimensions is relatively easy to implement, the lattices required to produce isotropic hydrodynamics in three dimensions are large, requiring the storage of a large amount of data per site, and more importantly, increasing the size of the lookup tables used to choose collision outcomes which conserve momentum. Since the occupation of each site is an integer (usually one or zero), the technique is noisy, and much averaging must be performed to produce useful results; such averaging can itself consume a large amount of computing time.

1.2 The Lattice Boltzmann Equation

Although a Boltzmann equation formulation of LGA had been used often to treat the model analytically, it was not until 1988 that McNamara and Zanetti[32] suggested solving the lattice Boltzmann equation directly, and computing successive values of the real-valued single-particle distribution function $f_i(\mathbf{r}, t)$, rather than finding its value through computationally-intensive averaging of a lattice gas model. McNamara and Zanetti's model used a collision operator derived from a variant of the FHP lattice gas described by d'Humières and Lallemand[33]. The collision operator contained polynomials in f_i with as many terms as there were effective collisions; this was sufficiently complicated to work with that the model was never generalized to three dimensions.

Higuera *et al* [34, 35] suggested a method for obtaining simplified linear collision operators, which could be generalised to three dimensions. However, these models were still plagued by the density-dependent factor $g(\rho)$ seen in LGA.

1.2.1 Lattice BGK

That the collision term in lattice Boltzmann models was the cause of difficulties should not be surprising; the collision integral in the continuum lattice Boltzmann equation is not particularly easy to work with either.

However, an H-theorem exists for the continuum Boltzmann equation, requiring the single-particle distribution function $f(\mathbf{r}, t)$ it describes to evolve towards a well-defined equilibrium value $f^{(\mathrm{eq})}(\mathbf{r}, t)$. In the light of this, Bhatnagar, Gross, and Krook[36] suggested that a reasonable approximation to the continuum collision integral Ω would be a term describing the linear relaxation of the distribution function towards its equilibrium value, at a rate controlled by a single relaxation time parameter, τ :

$$\Omega \simeq \frac{f^{(\mathrm{eq})} - f}{\tau} \tag{1.18}$$

An analogous modification to the lattice Boltzmann equation was performed independently by Qian *et al*[37], and Chen *et al*[38, 39], approximating the collision operator to produce what is now commonly referred to as the "lattice BGK equation":

$$f_i(\mathbf{r} + \mathbf{c}_i, t + 1) - f_i(\mathbf{r}, t) = -\frac{1}{\tau}\left[f_i(\mathbf{r}, t) - \bar{f}_i(\mathbf{r}, t)\right] \tag{1.19}$$

In continuum Boltzmann equation treatments, the equilibrium distribution can be found from the lower bound of the H-theorem. In introducing the BGK approximation, Qian *et al* simply used the equilibrium distribution for the Boltzmann equation describing a lattice gas; note, however, that this is *not* necessarily the thermodynamic equilibrium distribution function for a lattice Boltzmann model, which is a different dynamical system.

This is a point which was not made terribly clear in the early literature surrounding lattice BGK – the "equilibrium" value $\bar{f}_i$ towards which the distribution function f_i relaxes is an equilibrium value in the sense that if f_i ever takes the exact value $\bar{f}_i$ at all points on the lattice, then the system will cease to evolve in time. However, essentially all interesting LBE models lack detailed balance or H-theorems[40]: in the absence of these, there is no guarantee that f_i will ever attain the value $\bar{f}_i$.

Qian also developed a method for making certain anisotropic lattices produce isotropic hydrodynamics, by introducing a weighting factor T_i for each lattice vector $\mathbf{c}_i$, with the result that the lattice tensors are redefined to be

$$T^{(n)}_{\alpha_1\ldots\alpha_n} \doteq \sum_i T_i c_{i\alpha_1}\cdots c_{i\alpha_n} \tag{1.20}$$

For the lattices enumerated in the paper by Qian, d'Humières and Lallemand[37], the redefined lattice tensor (1.20) obeys the isotropy requirements (1.14–1.17).

The lattice gas Boltzmann equation equilibrium distribution N_i for these lattices was found[41] to be given in terms of the velocity $\mathbf{u}$ and number density $n = \rho/m$ of particles at a site, by

$$N_i = nT_i\left[1 + \frac{c_{i\alpha}u_\alpha}{c_s^2} + \frac{u_\alpha u_\beta}{2c_s^2}\left(\frac{c_{i\alpha}c_{i\beta}}{c_s^2} - \delta_{\alpha\beta}\right)\right] \tag{1.21}$$

By multiplying and summing over lattice vectors according to the relations (1.10,1.11), and using the property of lattice isotropy (1.14–1.17) to simplify the lattice tensors, it can easily be seen that this equilibrium distribution conserves the mass and momentum of colliding particles:

$$\sum_i N_i = n\left[\left(1 - \frac{1}{2c_s^2}u_\alpha u_\beta\right)\sum_i T_i + \frac{1}{c_s^2}u_\alpha T^{(1)}_\alpha + \frac{1}{2c_s^2}u_\alpha u_\beta T^{(2)}_{\alpha\beta}\right] = n \tag{1.22}$$

$$\sum_i N_i c_{i\alpha} = n\left[\left(1 - \frac{1}{2c_s^2}u_\alpha u_\beta\right)T^{(1)}_\alpha + \frac{1}{c_s^2}u_\alpha T^{(2)}_{\alpha\beta} + \frac{1}{2c_s^2}u_\alpha u_\beta T^{(3)}_{\alpha\beta\gamma}\right] = nu_\alpha \tag{1.23}$$

Note the additional requirement that $\sum_i T_i = 1$.

The resulting "lattice BGK" model had substantial improvements over lattice gas: it is less noisy, and therefore requires much less computationally-intensive averaging; it is much simpler to implement, since the algorithm is deterministic and does not require the use of various computational tricks to speed up the process of choosing the outcome of collisions. Moreover, the lattice BGK model described above is Galilean invariant, and does not have a velocity-dependent pressure, which were two considerable problems with lattice gases.

However, these advantages were obtained at the cost of going back to requiring the use of floating-point arithmetic, and at the cost of numerical instabilities reappearing in the model: unlike lattice gas, lattice BGK is not unconditionally stable.

Another factor contributing to the resulting popularity of the LBGK method is that the introduction of extra terms representing eternal forces or interactions between fluid particles is much easier than in lattice gas models. Several systems for introducing forcing into LBGK have been proposed, some of which contain a single term representing the force on a unit particle, which can then be set to whatever value is required. This ease is in contrast to lattice gas methods, where one is required to either shift the probability distribution of collision outcomes[25], or repopulate the lattice vectors at each timestep in such a way as to increase the nett momentum of the particles.[30]

It has more recently been shown, for example by He and Luo[42, 1] or Abe,[2] that the lattice BGK method may also be derived through a systematic discretization of the continuum Boltzmann BGK equation, completely independently of lattice-gas automata.

1.3 Immiscibility

In generalizations of the lattice Boltzmann model to more than one component, the single-particle distribution function f_i is replaced by a set of different distribution functions f_i^σ for each fluid component σ. In the absence of any direct link to real-life fluids, the components are usually referred to by a unique "colour" assigned to each component. The expressions for mass and velocity of a single component generalize in the obvious way: the mass density of a single component at a site is $m^\sigma \sum_i f_i^\sigma$, and its momentum $m^\sigma \sum_i f_i^\sigma \mathbf{c}_i$. Flekkøy[43] suggested a multiphase miscible lattice Boltzmann scheme in 1993, with a matrix collision operator; most work on multiphase flow since then has concentrated on lattice BGK.

1.3.1 The Rothman-Keller LBE Model

The Rothman-Keller model for immiscible lattice gases altered the probabilities of different collision outcomes to favour those which would bring about a separation of the fluid components. Gunstensen *et al*[44] suggested a lattice Boltzmann model based around the linearized matrix collision operator of McNamara and Zanetti:[32] specifically, they added a perturbation to the collision operator to produce an anisotropic pressure tensor near interfaces between two immiscible fluids while still conserving the total momentum; the outgoing collided particles were then recoloured to produce zero diffusivity of one colour into the other.

Laplace's law was verified for this model, and simulations of capillary waves were carried out. However, the model used the inefficient matrix collision operator, and could not handle two fluids with different densities and viscosities.[45]

Grunau *et al*[46] modified this model to take the BGK form, in a way that permitted variable densities and viscosities. The collision step still consisted of two stages: the first collided the particles according to the BGK operator(1.18); the second recoloured the outgoing particles in such a way as to maximize the outgoing colour flux, defined as

$$\mathbf{\Phi}(\mathbf{r}) = \sum_i \left[\rho^r(\mathbf{r}+\mathbf{c}_i) - \rho^b(\mathbf{r}+\mathbf{c}_i)\right]\mathbf{c}_i \tag{1.24}$$

The kinematic viscosity $\nu^\sigma$of a given pure phase in this model was a function only of its relaxation time τ^σ, allowing the simulation of fluids with differing viscosities. Exploiting this feature, they were able to reproduce fingering in a Hele-Shaw cell, when a less viscous fluid was forced to invade a more viscous fluid; a Laplace law verification was also performed.

1.3.2 The Shan-Chen Model

Shan and Chen[47] suggested another generalization of the lattice BGK model to multicomponent fluids with interactions. The form (1.21) of the equilibrium distribution function is retained, but a different velocity $\mathbf{v}^\sigma$ is used for each component, so that the kinetic equation obeyed by the model is

$$f_i^\sigma(\mathbf{r}+\mathbf{c}_i, t+1) - f_i^\sigma(\mathbf{r}, t) = -\frac{1}{\tau^\sigma}\left[f_i^\sigma(\mathbf{r}, t) - N_i^\sigma(\mathbf{v}^\sigma, t)\right] \tag{1.25}$$

It was assumed that, during each collision step, the velocities of each different phase quickly equalize in the absence of forces. The velocity v_α^σ of component σ used in the equilibrium distribution function was written as a sum of this equalized velocity u'_α, and a small increment due to the force $\mathbf{F}^\sigma$ acting on that component

$$v_\alpha^\sigma \doteq u'_\alpha + \frac{\tau^\sigma}{\rho^\sigma} F_\alpha^\sigma \tag{1.26}$$

The requirements were imposed that the mass of a given component is conserved, and that the change in total momentum at a given site is entirely due to the sum of all forces acting on the fluid mixture at that site.

$$\begin{aligned} m^\sigma \sum_i \Omega_i^\sigma &= 0 && (1.27)\\ \sum_\sigma m^\sigma \sum_i \Omega_i^\sigma c_{i\alpha} &= \sum_\sigma F_\alpha^\sigma && (1.28)\end{aligned}$$

This produces an expression for the equalized velocity u'_α.

$$u'_\alpha \doteq \left(\sum_\sigma \frac{\rho^\sigma}{\tau^\sigma} u_\alpha^\sigma\right) / \left(\sum_\sigma \frac{\rho^\sigma}{\tau^\sigma}\right) \tag{1.29}$$

The force $\mathbf{F}^\sigma$ can take arbitrary values, such as $g\rho^\sigma\hat{\mathbf{z}}$ to give a gravitational force acting in the z-direction. In order to produce nearest-neighbour interactions between components, Shan and Chen suggested a force taking the form

$$F_\alpha^\sigma(\mathbf{x}) = -\psi^\sigma(\mathbf{x}) \sum_{\bar\sigma} g_{\sigma\bar\sigma} \sum_i \psi^{\bar\sigma}(\mathbf{x}+\mathbf{c}_i) c_{i\alpha} \tag{1.30}$$

$\psi^\sigma(\mathbf{x}) = \psi^\sigma(\rho^\sigma(\mathbf{x}))$ is an effective mass for component σ; $g_{\sigma\bar{\sigma}}$ is a constant controlling the interaction between two different components.

In order to model immiscible fluids, ψ^σ may simply be set to ρ^σ; $g_{\sigma\bar{\sigma}}$ is set to zero for $\sigma = \bar{\sigma}$, and a positive value for $\sigma \neq \bar{\sigma}$: for a given component, this will produce a force in a direction directly away from any interfaces. Taylor-expanding the second effective-mass term in (1.30) gives

$$\psi^{\bar{\sigma}}(\mathbf{x} + \mathbf{c}_i) \simeq \psi^{\bar{\sigma}}(\mathbf{x}) + c_{i\beta}\partial_\beta \psi^{\bar{\sigma}}(\mathbf{x}) + \frac{1}{2} c_{i\beta} c_{i\gamma} \partial_\beta \partial_\gamma \psi^{\bar{\sigma}}(\mathbf{x}) + \dots \tag{1.31}$$

Substituting into (1.30), and using the expressions (1.14–1.17) to perform the summation over the lattice vectors $\mathbf{c}_i$ shows that, to second-order, the force acts in a direction opposite to the concentration gradient of the components.

$$\begin{aligned} F^\sigma_\alpha &= \psi^\sigma \sum_{\bar{\sigma}} g_{\sigma\bar{\sigma}} \sum_i \left(c_{i\alpha} + c_{i\alpha} c_{i\beta} \partial_\beta + \frac{1}{2} c_{i\alpha} c_{i\beta} \partial_\beta \partial_\gamma + \dots \right) \psi^{\bar{\sigma}} && (1.32) \\ &\simeq c_s^2 \psi^\sigma \sum_{\bar{\sigma}} g_{\sigma\bar{\sigma}} \partial_\alpha \psi^{\bar{\sigma}} && (1.33) \end{aligned}$$

The Shan-Chen model may also be used to describe liquid-gas mixtures: defining a nonzero $g_{\sigma\sigma}$ gives rise to a repulsive force between particles of the same phase[48]. A coexistence curve was determined for a simple liquid-gas mixture, and it was found that this curve agreed with the classic thermodynamic theory if the effective mass function was chosen to be $\psi(\rho) = \psi_0 \exp(-\rho_0/\rho)$ for arbitrary constants ψ_0,ρ_0. Comparisons of the immiscible-fluid model with existing theory are more difficult, since they have not been treated as successfully in theory.

Recently, Martys and Douglas[49] identified the immiscible-fluid coupling constant $g_{\sigma\bar{\sigma}}$ with a temperature-like parameter, finding a critical exponent of 1/2 for the composition of symmetric fluid mixtures as the coupling was reduced towards zero: in addition, they defined a temperature-like parameter by summing the kinetic energies of the particles at a given site:

$$T(\mathbf{x}, t) = \frac{\sum_\sigma m^\sigma \sum_i \bar{f}^\sigma_i(\mathbf{x}, t)(\mathbf{c}_i - \mathbf{u})^2}{3 \sum_\sigma f^\sigma_i(\mathbf{x}, t)} \tag{1.34}$$

This was used to relate the Shan-Chen model to mean-field theories of phase separation, and the Flory-Huggins model of polymer blends. However, it is not clear how meaningful this temperature-like term is, since the model does not conserve kinetic energy, nor is there a fluctuation-dissipation relationship, since there are no random fluctuations in the model.

Momentum flux and nonlocality

In most lattice-BGK models, momentum is conserved locally:

$$\sum_\sigma m^\sigma \sum_i \Omega_i^\sigma(\mathbf{r}) c_{i\alpha} = 0 \tag{1.35}$$

A distinguishing feature of the model of Shan and Chen is that interactions are *nonlocal*:- in the collision step, momentum is exchanged between adjacent sites, so that the total momentum is conserved. However, it then becomes unclear how to determine a fluid velocity from the lattice-BGK distribution function: in other LBGK models, the momentum at a site only changes in the advection part of a timestep, so that the momentum of the fluid may be unambiguously found from the first velocity moment of the distribution function.

In the Shan-Chen model, the momentum at a site is changed during both the advection step and the collision step, and it is not immediately clear how one should attempt to determine the macroscopic fluid velocity for a given timestep. The most appropriate[48, 50] method is to take the temporal midpoint between advection and collision. Since the collision step changes the momentum by an amount $\sum_\sigma \mathbf{F}^\sigma$, the macroscopic fluid velocity $\mathbf{U}$ is defined as

$$\rho U_\alpha \doteq \sum_\sigma m^\sigma \sum_i f_i^\sigma c_{i\alpha} + \frac{1}{2}\sum_\sigma F_\alpha^\sigma \tag{1.36}$$

Laplace's law was verified for the 2D version of this model in Shan and Chen's original paper; Hou *et al*[45] performed further such tests on both the Shan-Chen model, and Grunau's version of the Rothman-Keller model.

The RK model showed substantial unphysical spurious currents developing when a Laplace law test was performed; the maximum velocity of the spurious currents induced in the SC model were around a factor of two smaller, and the extent of the currents was also substantially smaller in the SC model. It was also noticed that the velocity field in the RK model still oscillated in the final stages of the simulation, whereas the SC model velocities were comparatively steady.

1.3.3 The Oxford Model

Swift *et al*[51] introduced a multiphase lattice Boltzmann model designed to produce a well-defined isothermal equation of state. They defined a free energy functional of the density n:

$$\Psi[n] = \int \frac{\kappa}{2}|\nabla n(\mathbf{r})|^2 + \psi(n(\mathbf{r}))\mathrm{d}\mathbf{r} \tag{1.37}$$

The first term, controlled by the constant κ, gives the contribution from any density gradients; the second describes the bulk free energy density. The pressure is defined by

$$p(\mathbf{r}) = n\frac{\delta\Psi}{\delta n} - \Psi = p_0 - \kappa n \nabla^2 n - \frac{\kappa}{2}|\nabla n|^2 \tag{1.38}$$

where $p_0 = n\psi'(n) - \psi(n)$ is the equation of state of the fluid. The equilibrium distribution $\bar{f}_i$ is then constructed to conserve mass and momentum, and to produce a pressure tensor of the form

$$P_{\alpha\beta}(\mathbf{r}) = p(\mathbf{r})\delta_{\alpha\beta} + \kappa\partial_\alpha n\partial_\beta n \tag{1.39}$$

This system has the considerable advantage that it is possible to directly choose parameters such as the surface tension, by choosing an appropriate form of the free energy Ψ, and is easily generalized to multiphase fluids[52].

Note, however, that a problem with this model is that the viscosity term in the macroscopic equations is not Galilean-invariant[53], an effect which is substantial in the presence of large density gradients.

"Top-down" versus "Bottom-up"

The Oxford model is often referred to as a "top-down" lattice Boltzmann model, since it imposes a macroscopic equilibrium free-energy functional; by contrast, the Shan-Chen model is a phenomenological "bottom-up" model, since the force term (1.30) is related to ideas of microscopic interactions between particles.

While the ease with which macroscopic parameters may be chosen and the theoretical convenience of the system minimizing an arbitrary free-energy functional are substantial advantages of top-down models, it should be pointed out that it is only in thermodynamic equilibrium that free energy functionals are minimized. Since may of the applications of lattice Boltzmann are to non-equilibrium dynamics, where the system may be far from the postulated equilibrium state, the free energy functional may not be useful.

While the validity of this argument against free-energy models may be questionable, since the whole lattice BGK technique revolves around allowing the system to relax towards an equilibrium value which is determined (although perhaps not in the most rigorous manner) from the outset, it is harder to criticize the argument that imposing a macroscopic free-energy functional will produce models which say very little about how microscopic interactions set about producing such a free energy in the first place; the bottom-up models are more satisfying in this sense, particularly with recent attempts to link them to mean-field theories.[49]

Moreover, no H-theorem has been proved for lattice BGK, and the algorithm is still prone to numerical instabilities: arguments about supposed equilibrium dynamics hold little weight when there are no guarantees that such states can ever be reached.

1.4 Amphiphilic fluids

Several lattice Boltzmann models have been proposed for modelling fluids containing a surfactant component in addition to other, immiscible, components. Chen *et al* [54] generalized the Shan-Chen model to include surfactants, by introducing a separate surfactant component which had a dipole moment: the mean dipole moment is recorded at each site. The dipole moment relaxes according to a BGK ansatz, and its equilibrium state is found using a Heisenberg Hamiltonian, similar to that used for magnetism. The forces acting between the scalar coloured particles and the dipoles can be found by regarding each dipole particle as containing two immiscible particles, separated by a small distance: Taylor-expanding the Shan-Chen force (1.30) will then produce the approximate forces experienced by each phase, due to dipole interactions.

The Oxford free-energy model was also generalized[55, 56] to include surfactant terms: however, no dipole moments are considered – instead, the surfactant component is constrained to seek out and sit at the interface between two other components. While this may be a useful technique for examining how the addition of amphiphile slows down the process of phase separation, the model cannot be used to examine many of the interesting phenomena which arise in solutions of amphiphile in one other component: in particular, Nekovee and Coveney[57] have reported observations of the spontaneous assembly of lamellar and cubic bicontinuous phases in a Shan-Chen model of surfactant-water mixtures.

1.5 Applications of lattice Boltzmann

Although lattice Boltzmann is still regarded as an emerging technique, it has seen a wide variety of applications, a few of which will be summarized here.

Qian and Orszag[58] suggested a lattice BGK model for reaction-diffusion systems – that is to say, systems governed by an equation of the form

$$\partial_t \rho^\sigma = \kappa^\sigma \partial_{\alpha\alpha} \rho^\sigma + F^\sigma(\rho) \tag{1.40}$$

κ is the diffusivity of component σ; F^σ is a reaction function resulting from some chemical reaction process. The competition between the reaction and diffusion processes can give rise to complicated spatial or temporal structures, many of which are of particular interest to biologists.[59] Qian and Orszag were able to produce asymptotic scaling exponents for a diffusion-driven reactive model where two components react together to produce a third. Chopard and Luthi[60] were able to produce the spatial structures known as Liesegang bands, using a lattice Boltzmann model.

Ladd[61] used a matrix collision operator lattice Boltzmann scheme coupled with Newtonian molecular dynamics to model the motion of colloidal suspensions: the lattice Boltzmann code was used to calculate the hydrodynamic pressure on the suspended particles, whose motion through the fluid was treated by integrating their Newtonian equations of motion. Since the lattice Boltzmann method has low statistical noise, Brownian fluctuations were also added. Ladd's method modeled the suspended particles as hollow rigid shells filled with fluid: this did not fully recover the dynamics of truly solid particles. Heemels *et al*[62] proposed a correction to the model which prevented the transfer of momentum to the fluid internal to the particles, recovering correct dynamics for the solid particles.

There have been many studies of flow in porous media using LBE: for example, Martys and Chen[63] used the Shan-Chen model to examine the change in contact angle of a fluid interface against a wall as the degree of wetting, controlled by a force term at wall sites, was changed; they also performed studies of flow through digitized porous media, by taking a $64 \times 64 \times 64$ subsection of a $224 \times 288 \times 288$ high-resolution microtomography image of Fontainebleau sandstone. The lattice spacing in their model corresponded to a length scale of around $7.5\mu m$ on the digitized rock. Physically reasonable results were obtained for the permeability of the rock sample as a function of the proportion of wetting fluid being driven through it. Similarly, Mantle *et al* [64] simulated single-phase flow through a packed bed of catalyst particles, using MRI to produce boundary conditions such as the pore space geometry. The lattice Boltzmann results compared favourably with measurements taken with MRI velocimetry, although the LBE model did not predict flow close to walls very accurately.

Various modifications to the rheology in LBE have been made: Qian and Deng[65] modified the equilibrium distribution function to contain a term which produced Kelvin-Voigt-like viscoelastic behaviour. Wagner and Scott[66] used an Oxford-model LBE to examine spinodal decomposition with two viscoelastic phases. In particular, they allowed simulations to run both with and without viscoelastic fluids, and then turned the viscoelasticity off for late-time domain growth. They showed that the late-time scaling state in spinodal decomposition is not unique, since the different early-time domain morphologies they produced gave rise to different late-time growth laws.

Denniston*et al* [67] proposed a free-energy lattice Boltzmann model for liquid crystals, where they defined a tensor order parameter at each site, representing the director field of a liquid crystal. This was coupled to the flow through a free-energy functional.

Finally, LBE has been used to model flow effects such as the Rayleigh-Taylor instability[68], cavity flow[69], phase separation under shear[70], granular flows[71], or vortex shedding[72]. There is considerable interest in modelling of turbulence[73] with LBE: recent attempts to generalize the model to arbitrary meshes[74, 75, 76] suggest that it is a promising method for use in aerodynamic studies in the automobile industry.

Chapter 2

Research Report

2.1 Lattice Boltzmann Implementations

Two Shan-Chen lattice Boltzmann computer codes were written: the first was a 3D ternary amphiphilic code using a projection of the 4D FCHC lattice. This code, effectively a parallel reimplementation of a Fortran algorithm by Hudong Chen, was written by the author as a vacation project during the summer of 1999, and is designed to run on highly parallel supercomputers such as the SGI Origin 2000 or Cray T3E; descriptions of the code are to be found in Nekovee *et al.*[77, 78]

The second LBE code was for two-dimensional binary immiscible systems, on the D2Q9 lattice. The main piece of code is a 1400-line ANSI C program was written, containing the core algorithm itself and auxiliary routines to initialize the simulation, implement boundary conditions, and take care of memory handling and file I/O. A set of smaller 200-line programs were then written, each corresponding to a particular type of simulation. For example, the small program `lbe2d-spinodal` takes command-line arguments to set the parameters for each component (mass, initial density, etc), and then calls routines in the main LBE code to set up and run the simulation. In this way, the rarely-changed LBE engine is kept separate from the often-changing code to initialize and run simulations, simplifying maintenance of the code.

The results from the simulation, such as plots of density in the simulation arena, are written in the well-known platform-independent XDR format[79], so that results from a simulation run on one type of computer may be manipulated on any other type of computer, without the need to worry about differing floating-point formats or endianness issues. Several small utility programs were also written, to generate statistics from the XDR data, and also to convert visible images to and from XDR data: this means that datafiles representing, for example, the density of a single component, can be viewed directly on screen, and also that initial conditions or obstacle geometries may be drawn by hand in any paint package, and converted to XDR to feed into the simulation.

The code was compiled and executed on the IRIX/MIPS4 , Linux/IA64 , Linux/IA32 , Linux/Sparc64 , Linux/alpha, FreeBSD/IA32 , Solaris/Sparc64 , and UNICOSmk/T3E platforms; it should be easily portable to any other UNIX-like platform.

2.2 Spinodal Decomposition

Spinodal decomposition is an ideal application for lattice Boltzmann, since it is not easily treatable in theory without resorting to very crude approximations, which often neglect either hydrodynamics or the effects of the interfaces between components. It is a process of interest to industry, since phase separation plays an important part in, for example, production of polyurethane foams.

Two fluids considered immiscible at room temperature will normally mix above some ordering temperature T_c, when the thermal noise swamps the repulsion between the two fluid components. If a mixture of the two fluids above T_c is forced or "quenched" below the ordering temperature, the fluids will separate; the separation process is known as spinodal decomposition. Much of the theory surrounding the process has been summarized by Bray[80] and Furukawa[81]; however, recent work has shown that the process is not as straightforward as these theoretical treatments may suggest.

A simple treatment of the process divides it into three main regimes: early-time diffusive growth, during which small density fluctuations grow to form interfaces between domains containing a single phase; a viscous hydrodynamic regime, where the coarsening of these domains is driven by surface-tension effects, and a late-time regime, where coarsening is driven by inertial hydrodynamic flow. Grant and Elder[82] also proposed the existence of a turbulent regime, where the flow is sufficiently strong to re-mix the fluid, preventing further domain growth. Theoretical treatments[81] suggest that a single length scale should exist at a given time in each of these regimes, and that this length scale varies as a power of the time; most models of LBE have attempted to determine these growth exponents. Most examinations of spinodal decomposition have found late-time inertial hydrodynamic growth exponents of $\frac{2}{3}$, in agreement with Furukawa's predictions, with early-time exponents of $\frac{1}{2}$ or $\frac{1}{3}$ in 2D and 1 in 3D. Although Grant and Elder proposed that the growth exponent should not exceed $\frac{1}{2}$ for sufficiently high Reynolds numbers, this regime has so far not been seen.

2.2.1 Previous LBE studies

Rothman-Keller models

Grunau *et al*[83] examined the separation of two immiscible phases in porous media with wetting walls. During the early stages of separation, when the phases had not completely separated, the domain growth was found to be independent of the wall characteristics; an early-time growth exponent of $\frac{1}{2}$ was found, followed by a late-time exponent of $\frac{2}{3}$. Chen and Lookman[84] examined separation of three or four immiscible components in 2D, using a model which introduced stochastic fluctuations to mimic the effect of finite temperature on the interface. They found a domain growth exponent of 0.4 ± 0.03; for three dimensions, they found an exponent of 0.96 ± 0.05 in agreement with the predictions of Siggia.[85] Curiously, the introduction of fluctuations was found to have no effect on the domain growth.

Rybka *et al* [86] used a Rothman-Keller model to find an early-time growth exponent of 0.33 ± 0.06, and a late-time exponent of 0.66 ± 0.06 for correlated quenches.

Free-energy model studies

Osborn *et al* [87] examined 2D spinodal decomposition in binary fluids with a free-energy model, and found early time exponents of $\frac{1}{2}$ for early times, and $\frac{2}{3}$ for late times. Cates *et al* [88, 89] examined spinodal decomposition in 3D, finding an early-time exponent of 1, and a late-time exponent of $\frac{2}{3}$.

Shan-Chen models

Although phase separation has been observed in Shan-Chen models[47], there have been no quantitative examinations of the domain growth. The 2D Shan-Chen LBE code was used to probe this area, and results were obtained which agreed with existing theories for the early-time diffusive regime and late-time inertial hydrodynamic regime. However, no observations of the viscous hydrodynamic regime have been made; it has been suggested[90] that this is because the crossover time at which inertial effects begin to dominate over diffusive effects occurs before the crossover between diffusive and viscous regimes.

2.2.2 Diffusive regime

Theory

A binary fluid may be described by a scalar order parameter $\phi(\mathbf{r})$ corresponding to the difference in densities of each component, at each site. The order parameter is zero at sites with both components in equal proportions, and becomes positive or negative in the demixing process.

During the very early stages of spinodal decomposition, the order parameter will be very small, and the system may be described by a linearized Cahn-Hilliard equation.[91].

For a symmetric binary fluid, assume that the potential energy V varies with the order parameter ϕ to give the famous double-well structure shown in figure 2.1. During the separation process, the order parameter will change from zero, to either ϕ^- or ϕ^+, corresponding to regions consisting entirely of the red phase, or entirely blue.

The Cahn-Hilliard equation describes the time evolution of the order parameter as a function of derivatives of the potential energy V. Conservation of particle number of each separate phase means that the order parameter must be conserved.

$$\frac{\partial \phi}{\partial t} = -M\nabla^2 \left[-\kappa \nabla^2 \phi + \frac{\partial V}{\partial \phi} \right] \tag{2.1}$$

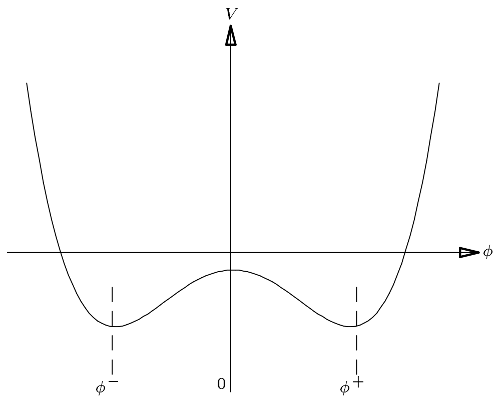

Figure 2.1: The potential energy of a mixture of two fluids as a function of the order parameter ϕ

At early times, the order parameter may be treated as a small perturbation about the initial value, so $\phi(t) = \phi_0 + u(t)$:

$$\frac{\partial u}{\partial t} = M\nabla^2 \left(-\kappa \nabla^2 + \left. \frac{\partial^2 V}{\partial \phi^2} \right|_{\phi_0} \right) u \tag{2.2}$$

At early times, the order parameter may be treated as a small For long wavelength disturbances, the fourth order spatial derivative may be neglected, hence

$$\frac{\partial u}{\partial t} \simeq M \left. \frac{\partial^2 V}{\partial \phi^2} \right|_{\phi_0} \nabla^2 u \tag{2.3}$$

At early times, the order parameter may be treated as a small This yields the diffusion equation, with diffusion constant:

$$D = M \left. \frac{\partial^2 V}{\partial \phi^2} \right|_{\phi_0} \tag{2.4}$$

At early times, the order parameter may be treated as a small For $\phi^- < \phi < \phi^+$, D is negative: particles are driven against the density gradient, in a process Cahn referred to as "uphill diffusion".

Consider the Fourier Transform of equation (2.2).

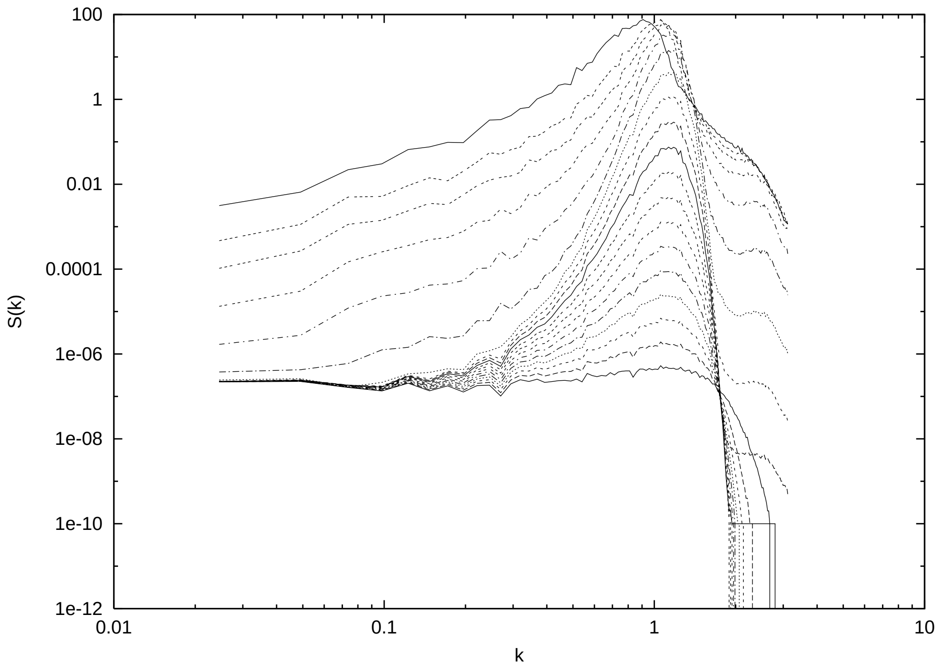

Figure 2.2: Circularly averaged structure function against wave vector (in inverse lattice sites), showing early-time exponential growth.

$$\frac{\partial}{\partial t}\tilde{u}(k,t) = -Mk^2\left(-\kappa k^2 + \left.\frac{\partial^2 V}{\partial \phi^2}\right|_{\phi_0}\right)\tilde{u}(k,t) = \omega(k)\tilde{u}(k,t) \qquad (2.5)$$

At early times, the order parameter may be treated as a small For wave-vectors less than some critical value k_c, the Fourier Transform of the order parameter grows exponentially in time:

$$k_c^2 = \frac{1}{\kappa}\left|\frac{\partial^2 V}{\partial \phi^2}\right|_{\phi_0} \qquad (2.6)$$

At early times, the order parameter may be treated as a small Simulations were carried out on a 256×256 lattice, whose sites were initially populated with a density of 1.0 ± 0.001 blue and 1.0 ± 0.001 red particles. Both components had a relaxation time $\tau^\sigma = 1.0$, and the immiscibility coupling constant $g_{\sigma\bar{\sigma}}$ was set to 0.07.

The size of domains in a system containing a scalar order parameter varying in space is often described by the structure function $S(\mathbf{k},t)$, defined for N lattice sites with a mean order parameter $\bar{\phi}$ as:

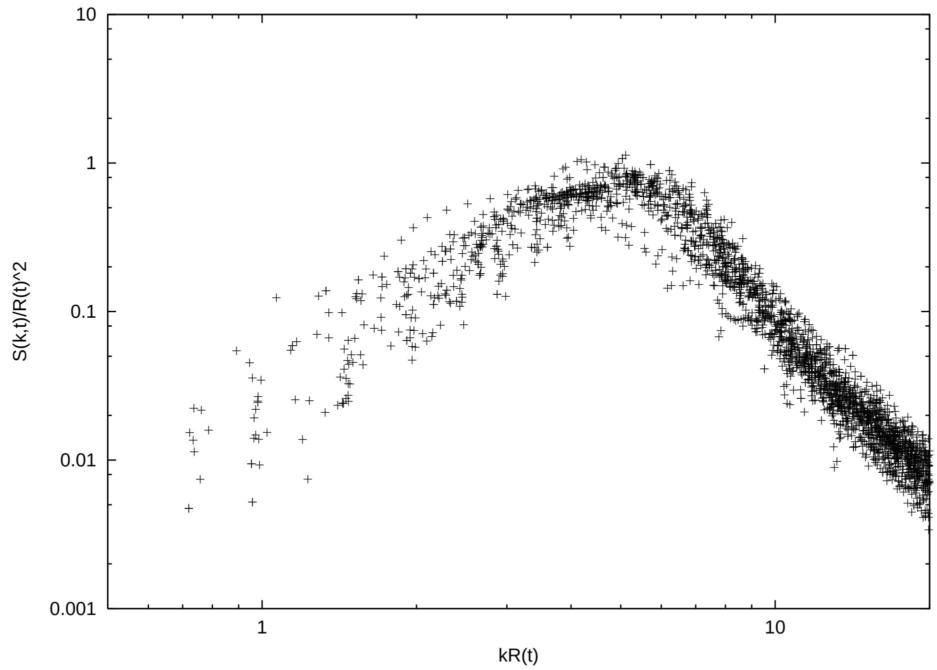

Figure 2.3: Rescaled structure function $S/R(t)^2$ plotted against $kR(t)$ (dimensionless), showing Porod tail.

$$S(\mathbf{k}, t) = \left\langle \frac{1}{N} \left| \sum_{\mathbf{r}} \left(\phi(\mathbf{r}) - \bar{\phi}\right) e^{i\mathbf{k}\cdot\mathbf{r}} \right|^2 \right\rangle \tag{2.7}$$

where angle brackets denote an ensemble average.

The circularly-averaged structure factor $S(k,t)$ was found to show exponential growth for long-wavelength fluctuations, until around timestep 80, when interfaces had formed, and surface tension and hydrodynamic effects overtook diffusive domain growth. Figure (2.2) shows the structure factor plotted every five timesteps from 5 to 95; after the interfaces have been formed, the peak in the structure factor begins to shift to lower values of k, corresponding to widening of the separated regions.

2.2.3 Hydrodynamic regime

For binary systems with sharp domain walls, the typical size $R(t)$ of a domain is often observed to obey a growth law of the form $R \sim t^n$. If R exceeds the hydrodynamic length $R_h = \frac{\nu^2}{\rho\sigma}$, then hydrodynamic effects dominate the coarsening, and it was predicted by Furukawa[81] that $n = \frac{2}{3}$ in this case.

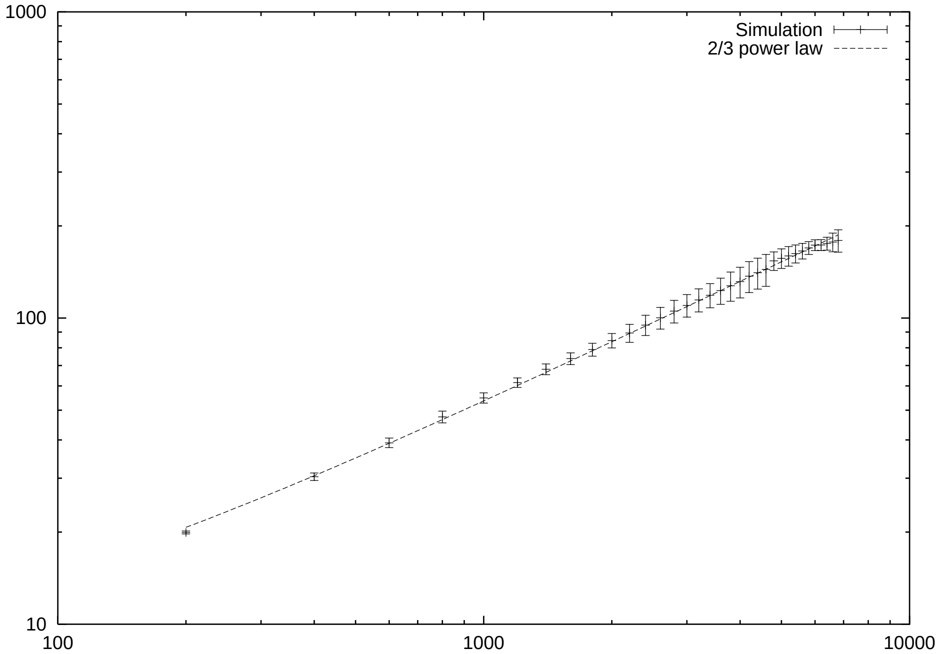

Figure 2.4: Inverse first moment of structure factor in lattice units against time in timesteps , showing late-time scaling.

Eight independent simulations runs were performed, each using different initial conditions of the form described above. The inverse first moment $R = \left(\int S(k)\mathrm{d}k\right) / \left(\int kS(k)\mathrm{d}k\right)$ of the radially averaged structure factor was chosen as a measure of the typical domain size, with averaging performed over the independent runs. A curve of the form $R = A(t - t_0)^n$ was fitted to the results, yielding $n = 0.636/pm0.007$, as can be seen in figure (2.4).

Figure (2.3) shows the rescaled structure function $F(x) = S/R(t)^2$ plotted against $x = kR(t)$. For $x > 5$, $F(x) \sim x^{-3.5}$, in reasonable agreement with Porod's law predicting $F(x) \sim x^{-(d+1)}$.

2.2.4 Breakdown of scaling

It is assumed in the above examinations of scaling behaviour that there exists a single typical length scale, which evolves in time; this is not necessarily the case, even for symmetric binary mixtures, as has been demonstrated experimentally by Tanaka[92], and in LBE simulations by Wagner and Yeomans[70]: for sufficiently low values of the diffusion constant, domains form quickly due to hydrodynamic effects, but this happens too quickly for the order parameter to attain its equilibrium value, leading to a second phase separation inside the domains.

The same effect has been observed with this model: using the parameter set $\tau = 1.8375$, $\rho = 1.8125$, $g = 0.05$, the system quickly separated into domains as shown in figure 2.5, with smaller circular domains appearing at later times, leading to a variety of length scales. There is no clear scaling behaviour when this effect occurs.

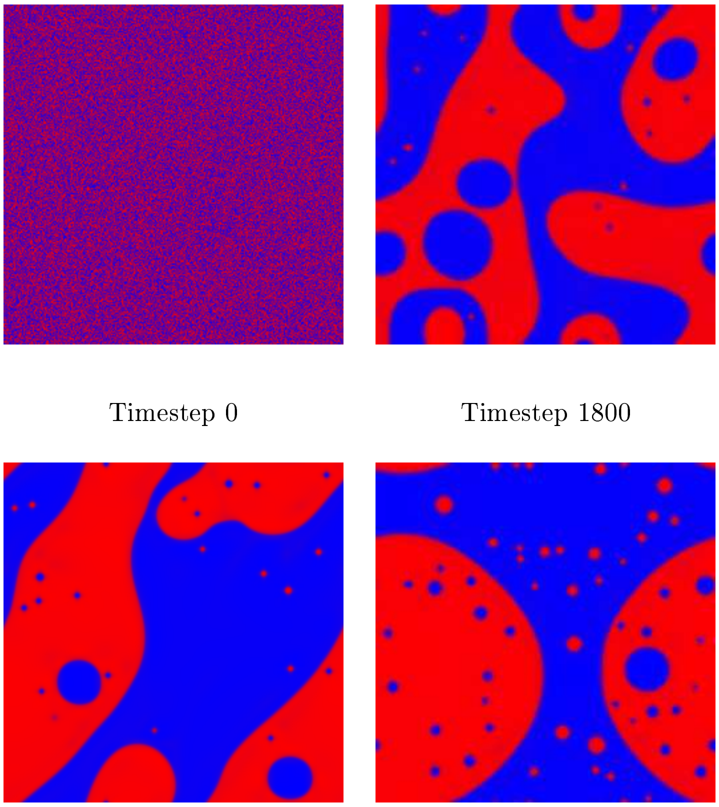

Timestep 0

Timestep 1800

Timestep 4000

Timestep 27200

Figure 2.5: Breakdown of scaling in 2D symmetric binary spinodal decomposition, showing the order parameter at different timesteps. Note the many different droplet sizes at late times.

2.3 Chapman-Enskog procedure for Shan-Chen model

In order to better understand the properties of the Shan-Chen model on different lattices, a Chapman-Enskog expansion was carried out for lattice BGK systems with the Shan-Chen force term, on the lattices defined by Qian *et al* [37]; most existing treatments[50, 93] of the Shan-Chen model have been restricted to the FHP or FCHC lattices.

The treatment below works for arbitrary numbers of immiscible or forced components, and is valid for *any* of the lattices defined by Qian *et al*; previous Chapman-Enskog procedures for the Shan Chen model seem to have been limited to specific lattices such as FHP, and produced macroscopic equations containing lattice-specific terms such as the number of nearest neighbours in single-velocity lattices. However, these may be absorbed into the speed of sound c_s^2, which in turn can be derived from the properties of the lattice – it turns out to be the coefficient of proportionality between the second order lattice tensor and the Kronecker delta, as can be seen in equation (1.15).

2.3.1 Moments of the equilibrium distribution

By multiplying N_i^σ by the appropriate number of lattice vectors $\mathbf{c}_i$, summing over i, and substituting the relations (1.14–1.17), the following moments of the equilibrium distribution can be found:

$$m^\sigma \sum_i N_i^\sigma(\mathbf{u}) = \rho^\sigma \tag{2.8}$$

$$m^\sigma \sum_i N_i^\sigma(\mathbf{u}) c_{i\alpha} = \rho^\sigma u_\alpha \tag{2.9}$$

$$m^\sigma \sum_i N_i^\sigma(\mathbf{u}) c_{i\alpha} c_{i\beta} = \rho^\sigma (c_s^2 \delta_{\alpha\beta} + u_\alpha u_\beta) \tag{2.10}$$

$$m^\sigma \sum_i N_i^\sigma(\mathbf{u}) c_{i\alpha} c_{i\beta} c_{i\gamma} = \rho^\sigma c_s^2 (u_\alpha \delta_{\beta\gamma} + u_\beta \delta_{\alpha\gamma} + u_\gamma \delta_{\alpha\beta}) \tag{2.11}$$

2.3.2 Power series expansion

The collision operator may be written as a Taylor expansion in time and space:

$$\begin{aligned}
\Omega_i^\sigma &= f_i^\sigma(\mathbf{r} + \mathbf{c}_i, t+1) - f_i^\sigma(\mathbf{r}, t) \\
&= (c_{i\alpha}\partial_\alpha + \partial_t) f_i^\sigma \\
&+ \frac{1}{2}(c_{i\alpha}\partial_\alpha + \partial_t)(c_{i\beta}\partial_\beta + \partial_t) f_i^\sigma \\
&+ \dots
\end{aligned}$$

In a Chapman-Enskog expansion, the distribution function is written as a power series expansion in a parameter ϵ.

$$f_i^\sigma \doteq f_i^{\sigma(0)} + \epsilon f_i^{\sigma(1)} + \epsilon^2 f_i^{\sigma(2)} + \ldots \tag{2.12}$$

This technique was originally used to derive the Navier-Stokes equations from the continuum Boltzmann equation, and ϵ was identified with the Knudsen number. Later treatments regarded ϵ as a variable thrown in to ensure that all terms of a given order are kept together: ϵ is later set to unity, similar to the treatment of perturbation theory in quantum mechanics. In many cases (including the remainder of this treatment), the ϵ is dropped from the equations altogether.

The time derivative is also written as a series expansion, with each term corresponding to a different physical timescale; spatial derivatives are treated as first-order.

$$\partial_t \doteq \partial_{1t} + \partial_{2t} + \ldots \tag{2.13}$$

Substituting these expansions into the Taylor series for the collision operator gives:

$$\begin{aligned}
\Omega_i^\sigma &= (c_{i\alpha}\partial_\alpha + \partial_{1t}) f_i^{\sigma(0)} \\
&+ (c_{i\beta}\partial_\beta + \partial_{1t}) f_i^{\sigma(1)} \\
&+ \left[\partial_{2t} + \frac{1}{2} c_{i\alpha}\partial_\alpha (c_{i\beta}\partial_\beta + \partial_{1t}) + \frac{1}{2}(c_{i\alpha}\partial_\alpha + \partial_{1t})\right] f_i^\sigma \\
&+ \ldots
\end{aligned}$$

Hence, $\Omega_i^\sigma = \Omega_i^{\sigma(1)} + \Omega_i^{\sigma(2)} + \ldots$, where

$$\Omega_i^{\sigma(1)} = (c_{i\alpha}\partial_\alpha + \partial_{1t}) f_i^{\sigma(0)} \tag{2.14}$$

$$\begin{aligned}
\Omega_i^{\sigma(2)} &= (c_{i\beta}\partial_\beta + \partial_{1t}) f_i^{\sigma(1)} \\
&+ \left[\partial_{2t} + \frac{1}{2} c_{i\alpha}\partial_\alpha (c_{i\beta}\partial_\beta + \partial_{1t}) + \frac{1}{2}(c_{i\alpha}\partial_\alpha + \partial_{1t})\right] f_i^{\sigma(0)}
\end{aligned} \tag{2.15}$$

In order to produce a set of macroscopic equations, the leading-order distribution function is set to be the equilibrium distribution about the macroscopic fluid velocity defined in (1.36), i.e.

$$f_i^{\sigma(0)} \doteq N_i(n^\sigma, \mathbf{U}) \tag{2.16}$$

Substituting $\mathbf{U}$ into the moments (2.8,2.9) of the equilibrium distribution function shows that the density and macroscopic momentum may be found from the first-order equilibrium distribution function:

$$m^\sigma \sum_i f_i^{\sigma(0)} = \rho^\sigma \tag{2.17}$$

$$\sum_\sigma m^\sigma \sum_i f_i^{\sigma(0)} c_{i\alpha} = \rho U_\alpha \tag{2.18}$$

However, the full distribution function (2.12) must still produce the single component density $m^\sigma \sum_i f_i^\sigma$ and kinetic momentum $m^\sigma \sum_i f_i^\sigma \mathbf{c}_i$: this requirement leads to restrictions on the higher-order terms in the expansion:

$$m^\sigma \sum_i f_i^{\sigma(n)} = 0 \qquad \text{for } n > 0 \tag{2.19}$$

$$\sum_\sigma m^\sigma \sum_i f_i^{\sigma(1)} c_{i\alpha} = -\frac{1}{2}\sum_\sigma F_\alpha^\sigma \tag{2.20}$$

$$\sum_\sigma m^\sigma \sum_i f_i^{\sigma(n)} c_{i\alpha} = 0 \qquad \text{for } n > 1 \tag{2.21}$$

For notational convenience, define the nth-order momentum flux tensors:

$$\begin{aligned}
\Pi_{\alpha_1\cdots\alpha_n}^{\sigma(\mathrm{n})} &\doteq m^\sigma \sum_i f_i^{\sigma(n)} c_{i\alpha_1}\cdots c_{i\alpha_n} \\
\Pi_{\alpha_1\cdots\alpha_n}^{\sigma} &\doteq \Pi^{\sigma(0)}_{\alpha_1\cdots\alpha_n} \\
\Pi_{\alpha_1\cdots\alpha_n} &\doteq \sum_\sigma \Pi_{\alpha_1\cdots\alpha_n}^{\sigma}
\end{aligned}$$

2.3.3 First-order macroscopic equations

Substituting the first order expansion (2.14) into the conservation relations (1.27,1.28) gives

$$\partial_\alpha \Pi_\alpha^\sigma + \partial_{1t}\rho^\sigma = 0 \tag{2.22}$$

$$\partial_\beta \Pi_{\alpha\beta} + \partial_{1t}\Pi_\alpha = \sum_\sigma F_\alpha^\sigma \tag{2.23}$$

Equation (2.22) describes the conservation of mass for a single component; equation (2.23) is an inviscid Euler equation for the fluid mixture, with a scalar, velocity-independent, pressure proportional to the density:

$$\partial_\alpha c_s^2 \rho + \partial_\beta \rho u_\alpha u_\beta + \partial_{1t}\rho u_\alpha = \sum_\sigma F_\alpha^\sigma \tag{2.24}$$

2.3.4 Second-order macroscopic equations

Continuity

Requiring continuity to second-order gives

$$\partial_\alpha \Pi_\alpha^{\sigma(1)} + \partial_{2t}\rho^\sigma + \frac{1}{2}\partial_\alpha\partial_\beta\Pi_{\alpha\beta}^\sigma + \partial_{1t}\partial_\alpha\Pi_\alpha^\sigma + \frac{1}{2}\partial_{1t}^2\rho^\sigma = 0 \tag{2.25}$$

Equation (2.22) can be differentiated to give $\partial_{1t}\partial_\alpha\Pi_\alpha^\sigma = -\partial_{1t}^2\rho^\sigma$; substituting into (2.25) gives

$$\partial_{2t}\rho^\sigma = -\partial_\alpha\Pi_\alpha^{\sigma(1)} - \frac{1}{2}\partial_\alpha\partial_\beta\Pi_{\alpha\beta}^\sigma + \frac{1}{2}\partial_{1t}^2\rho^\sigma \tag{2.26}$$

Summing over σ, then substituting (2.20) to get rid of the term in $\Pi_\alpha^{\sigma(1)}$ gives

$$\partial_{2t}\rho = \frac{1}{2}\partial_\alpha\sum_\sigma F_\alpha^\sigma - \frac{1}{2}\partial_\alpha\partial_\beta\Pi_{\alpha\beta} + \frac{1}{2}\partial_{1t}^2\rho \tag{2.27}$$

The terms on the right-hand side now cancel out upon substitution of equations (2.22) and (2.23), giving

$$\partial_{2t}\rho = 0 \tag{2.28}$$

Momentum

To second order, conservation of momentum gives:

$$\partial_\beta\Pi_{\alpha\beta}^{\sigma}{}^{(1)} + \partial_{1t}\Pi_\alpha^{\sigma(1)} + \partial_{2t}\Pi_\alpha^\sigma + \frac{1}{2}\partial_\beta\partial_\gamma\Pi_{\alpha\beta\gamma}^\sigma + \partial_{1t}\partial_\beta\Pi_{\alpha\beta}^\sigma + \frac{1}{2}\partial_{1t}^2\Pi_\alpha^\sigma = 0 \tag{2.29}$$

The first-order terms may be simplified by substituting the first-order terms in the BGK operator:

$$f_i^{\sigma(1)} = -\tau^\sigma(c_{i\gamma}\partial_\gamma + \partial_{1t})f_i^{\sigma(0)} \tag{2.30}$$

This gives

$$\Pi_\alpha^{\sigma(1)} = -\tau^\sigma\left[\partial_\beta\Pi_{\alpha\beta}^\sigma + \partial_{1t}\Pi_\alpha^\sigma\right] \tag{2.31}$$

$$\Pi_{\alpha\beta}^{\sigma}{}^{(1)} = -\tau^\sigma\left[\partial_\gamma\Pi_{\alpha\beta\gamma}^\sigma + \partial_{1t}\Pi_{\alpha\beta}^\sigma\right] \tag{2.32}$$

Substituting into the momentum equation (2.29) gives

$$\partial_{2t}\Pi_\alpha^\sigma = \left(\tau^\sigma - \frac{1}{2}\right)\partial_\beta\partial_\gamma\Pi_{\alpha\beta\gamma}^\sigma + \left(\tau^\sigma - \frac{1}{2}\right)\partial_{1t}^2\Pi_\alpha^\sigma + (2\tau^\sigma - 1)\,\partial_{1t}\partial_\beta\Pi_{\alpha\beta}^\sigma \tag{2.33}$$

Following, for example, Wolfram[22], the last two terms are dropped, since they become negligible for sufficiently small Mach number. This is not an entirely satisfactory move – Qian and Orszag [94] pointed out that they give rise to a term cubic in the velocity, whose magnitude relative to the other terms varies roughly as the square of the Mach number. Suggestions[95] have been made to correct for this effect.

Recombining the above equation with the first-order momentum equation (2.23), summing over components, and using $\partial_t \Pi_\alpha = \partial_{1t}\Pi_\alpha + \partial_{2t}\Pi_\alpha$ gives a Navier-Stokes equation for incompressible low Mach number flow:

$$\partial_t \Pi_\alpha + \partial_\beta \Pi_{\alpha\beta} = \sum_\sigma x^\sigma \left(\tau^\sigma - \frac{1}{2}\right) \partial_\beta \partial_\gamma \Pi_{\alpha\beta\gamma} + \sum_\sigma F_\alpha^\sigma \tag{2.34}$$

Here, the mass fraction of component σ is written as x^σ. This can be expanded to give

$$\partial_t U_\alpha + U_\beta \partial_\beta U_\alpha + \frac{1}{\rho}\left[\partial_\alpha (c_\mathrm{s}^2 \rho) - \sum_\sigma F_\alpha^\sigma\right] = \nu \partial_\beta \partial_\beta U_\alpha \tag{2.35}$$

The kinematic viscosity ν is given by

$$\nu = c_\mathrm{s}^2 \sum_\sigma x^\sigma \left(\tau^\sigma - \frac{1}{2}\right) \tag{2.36}$$

The force term for immiscible fluids is usually treated by substituting its Taylor-expanded form (1.32). It is perhaps worth noting that the force acting between components is (to second order in the expansion) proportional to the concentration gradient because of the lattice isotropy: it is possible that expansion beyond second order may provide a method for treating surfactant interactions as well.

Chapter 3

Conclusions

A review of the literature surrounding the lattice Boltzmann mesoscale modelling technique has been presented, summarizing the historical development of the method and some of its applications. While LBE has many advantages over other techniques, such as its speed and versatility, its usefulness is constrained by the fact that it does not produce a well-defined Gibbsian equilibrium state, and can be numerically unstable.

Studies have been made of 2D spinodal decomposition: the results agree with certain theoretical predictions, although a regime where domain growth is dominated by viscous inertial effects was not observed. Breakdown of scale-invariance was also observed, agreeing with observations made using a different LBE model.

It was observed by Boghosian*et al* [96] that the move to lattice BGK models and descriptions at the single-particle distribution function level has effectively jettisoned any kinetic-level physics in the model. They proposed that LBE models could be constructed which possess a Lyapunov functional, analogous to an H-theorem, which would produce a well-defined equilibrium state, and also an unconditionally stable model. The investigation and generalization of this "entropic lattice Boltzmann" model to multiphase or forced flows could be a way out of some of the main restrictions of the LBE method.

Several areas have been singled out for the next phase of research, in addition to the examination of entropic LBE methods. Work is currently ongoing to measure the interfacial surface tension in a Shan-Chen LBE model; this will assist other work, including an examination of viscous fingering effects in forced flow. An alternative procedure for "calibrating" the lattice Boltzmann method would be to determine a relationship between the Shan-Chen force and molecular parameters, perhaps by comparison with molecular dynamics simulations.

Finally, the LBE codes themselves are constantly being updated: it is hoped to add the possibility of simulating flow under shear, as well as other boundary conditions.

Bibliography

[1] L. Luo, *Phys. Rev. Lett.*, 1998, **81**, 1618–1621.

[2] T. Abe, *J. Comp. Phys.*, 1997, **131**, 241–246.

[3] P. J. Hoogerbrugge, J. M. V. A. Koelman, *Europhys. Lett.*, 1992, **19(3)**, 155–160.

[4] P. Español, P. Warren, *Europhys. Lett.*, 1995, **30(4)**, 191–196.

[5] P. Español, *Phys. Rev. E*, 1995, **52(2)**, 1734–1742.

[6] L. E. Reichl, *A Modern Course in Statistical Physics*, second edition, J. Wiley and Sons, 1972.

[7] C. A. Marsh, G. Backx, M. H. Ernst, *Phys. Rev. E*, 1997, **56(2)**, 1676–1691.

[8] P. V. Coveney, P. Español, *J. Phys. A: Math. Gen.*, 1997, **30**, 779–784.

[9] C. A. Marsh, P. V. Coveney, *J. Phys. A: Math. Gen.*, 1998, **31**, 6561–6568.

[10] P. V. Coveney, K. E. Novik, *Phys. Rev. E*, 1996, **54(5)**, 5134–5141.

[11] S. I. Jury, *Computer Simulation of Complex Fluids using Dissipative Particle Dynamics*, Ph.D. thesis, University of Edinburgh, 1999.

[12] S. Jury, P. Bladon, M. Cates, S. Krishna, M. Hagen, N. Ruddock, P. Warren, *Phys. Chem. Chem. Phys.*, 1999, **1**, 2051–2056.

[13] E. S. Boek, P. V. Coveney, H. N. W. Lekkerkerker, P. van der Schoot, *Phys. Rev. E*, 1997, **55(3)**, 3124–3133.

[14] P. Español, *Phys. Rev. E*, 1998, **57(3)**, 2390–2948.

[15] E. G. Flekkøy, P. V. Coveney, G. D. Fabritiis, *Phys. Rev. E*, 2000, **62(2)**, 2140–2157.

[16] A. Malevanets, R. Kapral, *Europhys. Lett.*, 1998, **44(5)**, 552–558.

[17] A. Malevanets, R. Kapral, *J. Chem. Phys.*, 1999, **110(17)**, 8605–8613.

[18] Y. Hashimoto, Y. Chen, H. Ohashi, *Comp. Phys. Comm.*, 2000, **129(1–3)**, 56–62.

[19] T. Sakai, Y. Chen, H. Ohashi, *Comp. Phys. Comm.*, 2000, **129(1–3)**, 75–81.

[20] A. Malevanets, J. M. Yeomans, *Europhys. Lett.*, 2000, **52(2)**, 231–237.

[21] U. Frisch, B. Hasslacher, Y. Pomeau, *Phys. Rev. Lett.*, 1986, **56(14)**, 1505–1508.

[22] S. Wolfram, *J. Stat. Phys.*, 1986, **45(3/4)**, 471–526.

[23] S. Chapman, T. G. Cowling, *The Mathematical Theory of Non-uniform Gases*, second edition, Cambridge University Press, 1952.

[24] U. Frisch, D. d'Humières, B. Hasslacher, P. Lallemand, Y. Pomeau, J.-P. Rivet, *Complex Systems*, 1987, **1**, 649–707.

[25] D. H. Rothman, J. M. Keller, *J. Stat. Phys.*, 1988, **52(3–4)**, 1119–1127.

[26] B. M. Boghosian, P. V. Coveney, *Comp. Phys. Comm.*, 2000, **129(1–3)**, 46–55.

[27] B. M. Boghosian, P. V. Coveney, A. N. Emerton, *Proc. Roy. Soc. Lond. A*, 1996, **452**, 1221–1250.

[28] A. N. Emerton, P. V. Coveney, B. M. Boghosian, *Phys. Rev. E*, 1997, **56(1)**, 1286–1306.

[29] A. N. Emerton, F. W. J. Weig, P. V. Coveney, B. M. Boghosian, *J. Phys. Condens. Matter*, 1997, **9**, 8893–8905.

[30] J. F. Olson, D. H. Rothman, *J. Fluid Mech.*, 1997, **341**, 343–370.

[31] P. V. Coveney, J. Maillet, J. L. Wilson, P. W. Fowler, O. Al-Mushadani, B. M. Boghosian, *Int. J. Mod. Phys. C*, 1998, **9(8)**, 1479–1490.

[32] G. R. McNamara, G. Zanetti, *Phys. Rev. Lett.*, 1988, **61(20)**, 2332–2335.

[33] D. d'Humières, P. Lallemand, *Complex Systems*, 1987, **1**, 599–632.

[34] P. J. Higuera, S. Succi, R. Benzi, *Europhys. Lett.*, 1989, **9(4)**, 345–349.

[35] F. J. Higuera, J. Jiménez, *Europhys. Lett.*, 1989, **9(7)**, 663–668.

[36] P. L. Bhatnagar, E. P. Gross, M. Krook, *Phys. Rev.*, 1954, **94(3)**, 511–525.

[37] Y. H. Qian, D. d'Humières, P. Lallemand, *Europhys. Lett.*, 1992, **17(6)**, 479–484.

[38] S. Chen, H. Chen, D. Martínez, W. Matthaeus, *Phys. Rev. Lett.*, 1991, **67(27)**, 3776–3779.

[39] H. Chen, S. Chen, W. H. Matthaeus, *Phys. Rev. A*, 1992, **45(8)**, 5339–5341.

[40] P. V. Coveney, private communication.

[41] Y. H. Qian, *Gaz sur Réseax at Théorie Cinétique sur Réseaux Appliquée à l'Equation de Navier-Stokes*, Ph.D. thesis, École Normale Supérieure, 1990.

[42] X. He, L.-S. Luo, *Phys. Rev. E*, 1997, **56(6)**, 6811–6817.

[43] E. G. Flekkøy, *Phys. Rev. E*, 1993, **47(6)**, 4247–4257.

[44] A. K. Gunstensen, D. H. Rothman, S. Zaleski, G. Zanetti, *Phys. Rev. A*, 1991, **43(8)**, 4320–4327.

[45] S. Hou, X. Shan, Q. Zou, G. Doolen, W. Soll, *J. Comp. Phys.*, 1997, **138**, 695–713.

[46] D. Grunau, S. Chen, K. Eggert, *Phys. Fluids A*, 1993, **5(10)**, 2557–2651.

[47] X. Shan, H. Chen, *Phys. Rev. E*, 1993, **47(3)**, 1815–1819.

[48] X. Shan, H. Chen, *Phys. Rev. E*, 1994, **49(4)**, 2941–2948.

[49] N. S. Martys, J. F. Douglas, *Phys. Rev. E*, 2001, **6(031205)**.

[50] X. Shan, G. Doolen, *J. Stat. Phys.*, 1995, **81(112)**, 379–393.

[51] M. R. Swift, W. R. Osborn, J. M. Yeomans, *Phys. Rev. E*, 1995, **75(5)**, 830–833.

[52] E. Orlandini, M. R. Swift, J. M. Yeomans, *Europhys. Lett.*, 1995, **32(6)**, 463–468.

[53] M. R. Swift, E. Orlandini, W. R. Osborn, J. M. Yeomans, *Phys. Rev. E*, 1996, **54(5)**, 5041–5052.

[54] H. Chen, B. M. Boghosian, P. V. Coveney, *Proc. Roy. Soc. Lond. A*, 2000, **456**, 2043–2047.

[55] O. Theissen, G. Gompper, D. M. Kroll, *Europhys. Lett.*, 1998, **42**, 419–414.

[56] A. Lamura, G. Gonnella, J. M. Yeomans, *Europhys. Lett.*, 1999, **45(3)**, 314–320.

[57] M. Nekovee, P. V. Coveney, Lattice Boltzmann simulations of self assembly of binary amphiphilic fluid into ordered lamellar and bicontinous cubic phases, submitted for publication: also found under `cond-mat/0101379` in Los Alamos Preprint Archive – `http://www.arXiv.org/` .

[58] Y. H. Qian, S. A. Orszag, *J. Stat. Phys.*, 1995, **81(1–2)**, 237–253.

[59] A. J. Koch, H. Meinhardt, *Rev. Mod. Phys.*, 1994, **66(4)**.

[60] B. Chopard, P. Luthi, M. Droz, *Phys. Rev. Lett.*, 1994, **72(9)**, 1384–1387.

[61] A. J. C. Ladd, *Phys. Rev. Lett.*, 1993, **70(9)**, 1339–1342.

[62] M. W. Heemels, M. H. J. Hagen, C. P. Lowe, *J. Comp. Phys.*, 2000, **164(1)**, 48–61.

[63] N. S. Martys, H. Chen, *Phys. Rev. E*, 1996, **53(1)**, 743–750.

[64] M. D. Mantle, A. J. Sederman, L. F. Gladden, *Chem. Eng. Sci.*, 2001, **56(2)**, 523–529.

[65] Y.-H. Qian, Y.-F. Deng, *Phys. Rev. Lett.*, 1997, **79(14)**, 2742–2745.

[66] A. . J. Wagner, C. E. Scott, in *Polymer Processing Society 16th Annual Meeting, Shanghai*, 2000 .

[67] C. Denniston, E. Orlandini, J. M. Yeomans, *Europhys. Lett.*, 2000, **52(4)**, 481–487.

[68] X. He, R. Zhang, S. Chen, G. D. Doolen, *Phys. Fluids*, 1999, **11(5)**, 1143–1152.

[69] S. Hou, Q. Zou, S. Chen, G. Doolen, A. Cogley, *J. Comp. Phys.*, 1995, **118**, 329–347.

[70] A. J. Wagner, J. M. Yeomans, *Phys. Rev. Lett.*, 1998, **80(7)**, 1429–1432.

[71] M. L. Tan, Y. H. Qian, I. Goldhirsch, S. A. Orszag, *J. Stat. Phys.*, 1995, **81(1–2)**, 87–103.

[72] X. He, G. Doolen, *Phys. Rev. E*, 1997, **56(1)**, 434–440.

[73] C. M. Teixeira, *Int. J. Mod. Phys. C*, 1998, **9(8)**, 1159–1175.

[74] X. He, G. Doolen, *J. Comp. Phys.*, 1997, **134(2)**, 306–315.

[75] X. He, L.-S. Luo, M. Dembo, *J. Comp. Phys.*, 1996, **129(2)**, 357–363.

[76] G. Peng, H. Xi, C. Duncan, S.-H. Chou, *Phys. Rev. E*, 1999, **59(4)**.

[77] M. Nekovee, J. Chin, P. V. Coveney, in *Proceedings of the Simulation 99 UCLse/UK Conference on Simulation*, 1999 .

[78] M. Nekovee, J. Chin, N. González-Segredo, P. V. Coveney, in *Proceedings of the Fourth UNAM Supercomputing Conference, Singapore*, 1999 .

[79] R. Srinivasan, XDR: External Data Representation Standard, Network working group request for comments: 1832, Internet Engineering Task Force, 1995, `http://www.ietf.org/rfc/rfc1832.txt`.

[80] A. J. Bray, *Adv. Phys.*, 1994, **43(3)**, 357–459.

[81] H. Furukawa, *Adv. Phys.*, 1985, **34(6)**, 703–750.

[82] M. Grant, K. R. Elder, *Phys. Rev. Lett.*, 1999, **82(1)**, 14–16.

[83] D. W. Grunau, T. Lookman, S. Y. Chen, A. S. Lapedes, *Phys. Rev. Lett.*, 1993, **71(25)**, 4198–4201.

[84] S. Chen, T. Lookman, *J. Stat. Phys.*, 1995, **81**, 223–235.

[85] E. D. Siggia, *Phys. Rev. A*, 1979, **20(2)**, 595–605.

[86] R. B. Rybka, M. Cieplak, D. Salin, *Physica A*, 1995, **222**, 105–118.

[87] W. R. Osborn, E. Orlandini, M. R. Swift, J. M. Yeomans, J. R. Banavar, *Phys. Rev. Lett.*, 1995, **75(22)**, 4031–4034.

[88] V. M. Kendon, J. C. Desplat, P. Bladon, M. E. Cates, *Phys. Rev. Lett.*, 1999, **83(3)**, 576–579.

[89] M. E. Cates, V. M. Kendon, P. Bladon, J. C. Desplat, *Faraday Disc.*, 1999, **112**, 1–11.

[90] P. J. Love, private communication.

[91] J. D. Gunton, M. S. Miguel, P. S. Sahni, in C. Domb, J. Lebowitz (eds.), *Phase transitions and Critical Phenomena*, volume 8, Academic Press New York, 1983 pp. 319–339, pp. 319–339.

[92] H. Tanaka, *Phys. Rev. Lett.*, 1994, **72(23)**, 3690–3693.

[93] X. Shan, G. Doolen, *Phys. Rev. E*, 1996, **54(4)**, 3614–3620.

[94] Y. H. Qian, S. A. Orszag, *Europhys. Lett.*, 1993, **21(3)**, 255–259.

[95] Y. H. Qian, Y. Zhou, *Europhys. Lett.*, 1998, **42(4)**, 359–364.

[96] B. M. Boghosian, J. Yepez, P. V. Coveney, A. Wagner, *Proc. Roy. Soc. Lond. A*, 2001, **457**, 717.